

Implementation of FSS substrate on microstrip patch antenna for terahertz communication

SELVAKUMAR GEORGE^{1,*}, V. NANDALAL², P. JEYAKUMAR³, S. VENKATESH BABU⁴

¹SCAD College of Engineering and Technology, Tirunelveli – 627414, India

²Sri Krishna College of Engineering and Technology, Coimbatore – 641008, India

³M.Kumrasamy College of Engineering, Karur- 639113, India

⁴Jaya College of Engineering and Technology, Chennai- 600056, India

The terahertz communication is highly attractive for high-speed data communication due to its large bandwidth. In this work, Frequency Selective Surfaces (FSS) -based patch antenna was designed for improving gain, bandwidth and directivity. Initially, square loop (SL) band stop FSS unit element was designed with a frequency range of 1.5 THz and the parameters are extracted by using MATLAB. Then the proposed FSS elements are converted into 9x9 square loop structures and embedded with the bottom of the patch. The simulation results show that the proposed FSS substrate patch antenna bandwidth is improved from 1230 GHz to 2260 GHz in the desired frequency band. The gain and directivity of an antenna were also improved by 3.73dBi. From the simulation results, it is observed that the proposed dual-layer FSS substrate-based patch antenna is suitable for 6G wireless networks.

(Received February 10, 2022; accepted August 10, 2022)

Keywords: Terahertz, Gain enhancement, Frequency selective surface, Band-stop

1. Introduction

Wireless technology has recently become quite popular and appealing for high-data-rate transmission with wide bandwidth. In addition, the high spectral efficiency and reliable transmission are extremely essential for future wireless technology which operated with Gigabits per second (Gbps) for single end-user as well as multi-users [1]. The aforementioned features will introduce spectrum congestion issues which can be overcome by multiple input multiple-output (MIMO) technology which increases the spatial multiplexing and system capacity [2,3]. Nowadays, the MIMO technology advancements are widely adapted in 5G networks which provide the data connection at the rate of Gbps for each user and the data traffic also increases rapidly in every base station [4]. The conventional microwave and millimeter wave-based communication systems are widely used in 5G networks in which huge data cannot be handled efficiently up to the end-user [5]. Alternatively, infrared communication is used for high-speed transmission but its performance diminishes with line-of-sight problems which means that the transmitter and receiver position needs to be aligned properly over a distance [6-8]. These limitations of the microwave, millimeter and infrared-based communication systems urge the researchers to use Tera Hertz (THz) waves for future 6G wireless networks which support huge data transmission [9]. In addition, the THz waves provide wide bandwidth, and their frequency range is 1000 times better for mobile communication when compared with other frequency spectrum [10-12]. Therefore, the THz frequency-based antenna is designed in the proposed work.

1.1. Related work

The microstrip antenna was designed in small dielectric material with a metal patch. This antenna has many attractive features such as lightweight, small size, easy manufacturing, wearable, and extremely appropriate massive volume production. In the literature survey, different categories of microstrip antennas were studied with single and dual bands by using various designs namely slotted, T-shape slotted and stacked type [13-19]. In addition, the microstrip antenna substrate is very thin as well as highly sensitive to various frequencies. Hence, current researchers mainly focused on the THz microstrip antenna which focused on the frequency range from 0.1 to 1 THz. Ge Zhang et al. designed the THz-frequency-based microstrip antenna by using a double-surface multichannel resonator. The antenna substrate on both surfaces is coupled with feed lines [13].

In general, the T-shaped structures are widely used for designing the dual-band microstrip antenna. Wang Haijun et al proposed a novel dual-band THz microstrip antenna and its working mechanism based on a dual T-shaped slit. The radiation gap of this antenna is modified by a metal patch which also alters the circuit path surface to realize the double frequency resonance at the lower THz region [14]. In addition, the similar kind of T-shaped THz antenna is designed by M. Khulbe et al, but the antenna gain is improved by the substrate volume [16]. These dual resonance-based T-shaped microstrip antennas were realized by epoxy resin (FR-4) substrate with symmetrical cutting copper-based coaxial feed slots which can provide high radiation efficiency and good directivity. [14,15].

The FR-4 substrate shows small absorption loss, low

cost, minor suppression, and good directivity to the human organ at the THz region, so it is very appropriate for manufacturing the wearable antennas [15]. Liton Chandra Paul et al., designed Photo Band Gap (PBG) antenna with defective ground assembly to build the microstrip antenna with large bandwidth. In this work, the rectangular microstrip is initially designed and then the PBG structure is used as the substrate. The device performance of this work is improved when compared with the previous one. After that defects are created in the ground plane and then it is optimized to achieve better results in terms of gain and bandwidth [16].

M. Saqib Rabbani et al. designed the antenna with a liquid crystal polymer substrate operated with various THz frequencies of 0.1, 0.635, and 0.835. This design was fabricated on a simple PCB board and used for various medical applications namely cancer detection by using THz spectroscopy [17]. G. Singh Brar et al. designed the stacked THz antenna with FR-4 substrate. The suppression effect principle is used for the semiconductor characteristic detection [18]. Prince et al. proposed the copper-based rectangular THz antenna with the slotted ground. The return loss of the antenna is very low, and the gain is 4.2 dB at the resonant frequency. This antenna is used for the detection of vitamins deficiency in biomedical applications [19]. Dual layer patch antennas integrated with metamaterial substrates as emitting components for THz biomedical imaging are presented in [20]. Furthermore, these THz antennas are used for numerous applications namely biomedical, radar, imaging, and highly secured data transmission.

In summary, there are various microstrip antennas were realized in the lower THz region. However, that kind of antenna development in the high-frequency band is still in the early stage. In addition, most of the antennas were designed with low gain, so the main issue of the THz antenna is a gain improvement [21]. Therefore, in this work Frequency Selective Surfaces (FSSs) based microstrip patch antenna is designed with enhanced gain, directivity, and bandwidth.

1.2. Main contributions

The following are the major contributions of the proposed work.

The ABCD parameters are used for the transmission and reflection coefficients extraction of the FSS array elements. We have designed the unit element of FSS, and the antenna performance is analyzed by using HFSS. Parametric analysis is carried out by using MATLAB.

Then, we have designed a dual-layer FSSs based patch antenna and its performance is analyzed using an HFSS simulator. Finally, the proposed patch antenna is compared with the existing THz patch antenna available in the recent literature.

The rest of the paper is organized as follows: The expression of ABCD parameters for the band stop SL-unit elements is presented in section 2. The design of a unit cell element-based simulation results is discussed in section 3. Dual-layer FSS-based microstrip patch antenna design is

explained in section 4. A comparison with previous research is done in section 5 and section 6 concludes the article.

2. Frequency selective surfaces

The FSS is the periodic planar medium that shows transmission/reflection property based on the frequency range. This medium mainly consists of a thin conducting element developed with the dielectric substrate. Generally, the FSS assembly is separated into the patch and aperture metallic element with a different dimensional arrangement. Depending on the geometry, FSS operated with four different modes: low pass, high pass, band pass, and band stop [22]. The FSS widely used in various fields namely antennas, military, wireless security, and medical application [23]. In [26], Anwar et al. highlights recent development on various FSS categories based on array element usage, structure design, fabrication procedures, applications, future prospects and difficulties. The FSS is designed with different shapes namely dipole, cross dipole, triple, square, Jerusalem cross, and ring structure [22]. The aforementioned result reveals that the single loop FSS shows the best result and works within different angles cross-polarization TE or TM modes, and slight band spacing. The Equivalent Circuit Model (ECM) is used to rapidly analyze the FSS performance with different dimensions. Therefore, this ECM model is used for FSS performance analysis.

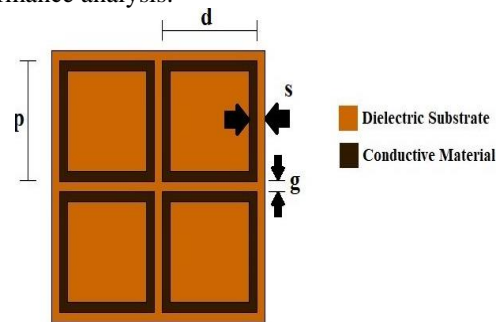


Fig. 1. An array of an FSS element (color online)

An array of SL-FSS element is shown in Fig. 1. The dimensions are summarized in Table 1.

Table 1. Description of the SL-shaped FSS unit elements

S.No	Symbol	Description	Value(m m)
1	p	Separation Period	0.1
2	d	Dimension of the loop	0.08
3	s	Width of the conducting strip	0.005
4	g	Inter-element spacing	0.02

The aforementioned parameters in Table 1 can control the resonant frequency. The FSS gap can control the angle performance [22]. The past study recommended that a larger loop size is normally effective at a low-frequency resonance and the small gap provide a stable resonance with different incident angle. The ECM method executes the interface between incident waves and the FSS which is

denoted by the wave propagation over the transmission link with a parallel impedance circuit. This impedance may be an inductor or capacitor depending on the incident angle polarization. From Fig. 2, the adjacent strips are moved toward one strip with $w=2S$ [22]. The normalized inductive reactance equation stated in [24].

$$X_{TE} = w_0 L / Z_0 \quad (1)$$

$$X_{TE} = \frac{p \cos \theta}{\lambda} \left[\ln \left(\csc \left(\frac{\pi w}{2p} \right) + G(p, w, \lambda, \theta) \right) \right] \quad (2)$$

$$X_{TM} = \frac{p \sec \theta}{\lambda} \left[\ln \left(\csc \left(\frac{\pi w}{2p} \right) + G(p, w, \lambda, \theta) \right) \right] \quad (3)$$

The normalized shunt capacitive susceptance expression was given by Lee [25].

$$B_{TM} = 4F(p, g, \lambda) = \frac{4p \cos \phi}{\lambda} \left[\ln \left(\csc \left(\frac{\pi g}{2p} \right) + G(p, g, \lambda, \phi) \right) \right] + \epsilon_{eff} \quad (6)$$

where G is the correction term

$$G(p, w, \lambda, \theta) = \frac{0.5(1-\beta^2)^2 \left[\left(1 - \frac{\beta^2}{4}\right)(A_{1+} + A_{1-}) \right] + 4\beta^2 A_{1+} A_{1-}}{\left(1 - \frac{\beta^2}{4}\right) + \beta^2 \left(1 + \frac{\beta^2}{2} - \frac{\beta^4}{8}\right)(A_{1+} + A_{1-}) + 2\beta^6 A_{1+} A_{1-}} \quad (7)$$

$$G(p, g, \lambda, \theta) = \frac{0.5(1-\beta^2)^2 \left[\left(1 - \frac{\beta^2}{4}\right)(A_{1+} + A_{1-}) \right] + 4\beta^2 A_{1+} A_{1-}}{\left(1 - \frac{\beta^2}{4}\right) + \beta^2 \left(1 + \frac{\beta^2}{2} - \frac{\beta^4}{8}\right)(A_{1+} + A_{1-}) + 2\beta^6 A_{1+} A_{1-}} \quad (8)$$

where

$$A_{1\pm}^{TE} = \frac{1}{\sqrt{\left(\frac{p \sin \theta}{\lambda} \pm 1\right)^2 - \frac{p^2}{\lambda^2}}} - 1 \quad (9)$$

$$A_{1\pm}^{TM} = \frac{1}{\sqrt{1 - \frac{p^2 \cos^2 \theta}{\lambda^2}}} - 1 \quad (10)$$

and

$$\beta = \sin 0.5 \pi w / p \quad (11)$$

or

$$\beta = \sin \frac{0.5 \pi g}{p} \quad (12)$$

where λ is the wavelength, θ is the incidence angle, $Z_0 = 377$, and ϵ_{eff} is the dielectric substrate's effective permittivity. The equation 8 shows the FSS output as a function of dimension, incident angle, and dielectric material. Furthermore, the mentioned equation is effective with $[p(1 + \sin \theta) < \lambda]$ for TE wave and $[p \cos \theta < \lambda]$ for TM wave for the incident angle. The equivalent impedance of the SL FSS is given by:

$$Z_{FSS} = j \left(X_L - \frac{1}{B_C} \right) \quad (13)$$

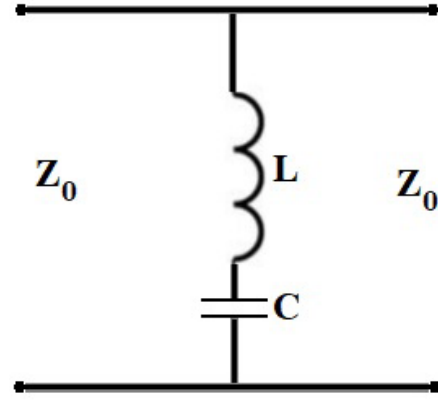


Fig. 2. The equivalent circuit of the band stop FSS SL-element

$$B_{TE} = w_0 C / Y_0 \quad (4)$$

$$= \frac{4p \sec \theta}{\lambda} \left[\ln \left(\csc \left(\frac{\pi g}{2p} \right) + G(p, w, \lambda, \theta) \right) \right] + \epsilon_{eff} \quad (5)$$

Therefore, the transmission line normalized impedance is illustrated in Fig. 3 and determined by:

$$Z_n = \frac{Z_{FSS}}{Z_0} = j \left(\frac{X_L}{Z_0} - \frac{1}{B_C Z_0} \right) = j \left(\frac{X_L}{Z_0} - \frac{Y_0}{B_C} \right) \quad (14)$$

The ABCD matrix is used to determine the FSS coefficient for signal transmission and reflection. Based on the ABCD parameters, the transmission (S_{21}) and the reflection coefficient (S_{11}) are calculated [22]. For instance, the T-network as shown in Fig. 3 and its matrix is described by:

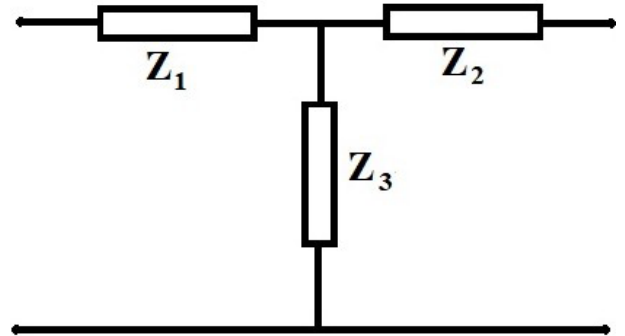


Fig. 3. Transmission line represented by ABCD matrix

$$\begin{bmatrix} A & B \\ C & D \end{bmatrix} = \begin{bmatrix} 1 + \frac{Z_1}{Z_3} & Z_1 + Z_2 + \frac{Z_1 Z_2}{Z_3} \\ \frac{1}{Z_3} & 1 + \frac{Z_2}{Z_3} \end{bmatrix} \quad (15)$$

$$\begin{bmatrix} S_{11} & S_{12} \\ S_{21} & S_{22} \end{bmatrix} = \begin{bmatrix} \frac{A+B-C-D}{\Delta} & \frac{2(AD-BC)}{\Delta} \\ \frac{2}{\Delta} & \frac{-A+B-C+D}{\Delta} \end{bmatrix} \quad (16)$$

where, $\Delta = A + B + C + D$. For the SL FSS, $Z_1 = Z_2 = 0$ and $Z_3 = Z_n$ as defined in Eq. (16). Therefore, based on Eq. (17) and Eq. (18), the transmission coefficient S_{21} and reflection coefficient S_{11} for the FSS can be evaluated. Because of symmetry $S_{11} = S_{22}$ and $S_{12} = S_{21}$. The ABCD matrix can be expressed as a function of S_{21} and S_{11} as:

$$S_{21} = \frac{2}{A+B+C+D} = \frac{2}{1+0+\frac{1}{Z_3}+1} = \frac{2}{2+\frac{1}{Z_3}} = \frac{2}{2+Y} = T \quad (17)$$

$$S_{11} = \tau = 1 - |T|^2 = 1 - \frac{4}{4+Y^2} \quad (18)$$

3. FSS Unit Element Design

The FSS unit cell geometry is shown in Fig. 4. It consists of SL shaped metallic structure imprinted on the bottom of the substrate which is made of silicon with a dielectric constant of 11.9 and thickness is 0.04 mm. The unit-cell separation period is 0.1 mm. The loop size is 0.08 mm and metallic strip width is 0.005mm and the elements gap is 0.02 mm. The proposed unit cell simulation was carried out using HFSS Simulator.

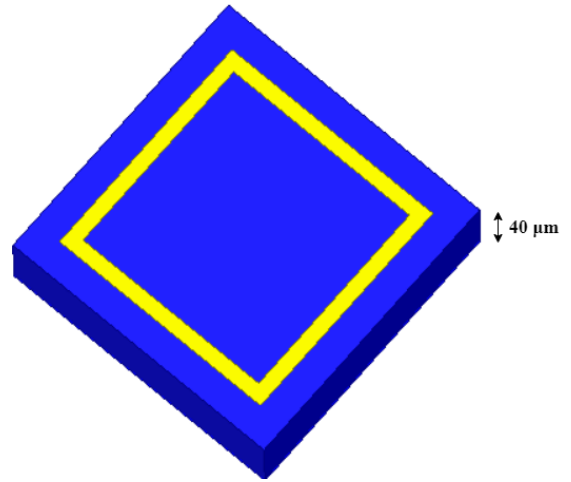


Fig. 4. Front view of stop band unit cell (color online)

MATLAB is used to extract the permittivity and permeability of the SL-FSS structure from the transmission and reflection coefficient. The SL shaped FSS structure has the reflection coefficient (S_{11}) of -50.49, -43.06 and -58.92 at three stop band at 2.33 THz, 3.07 THz and 6.11 THz respectively as shown in Fig.5. The Transmission coefficient (S_{21}) is extracted from equation (17), which shows how much power is transferred from input to output port. For proposed work, the transmission coefficient is observed as -104.03 and -107.34 at 1.4 THz and 1.97 THz respectively as shown in Fig. 6. The FSS unit element permeability, permittivity, refractive index and impedance were calculated from the S parameter by using MATLAB as shown in Fig. 7.

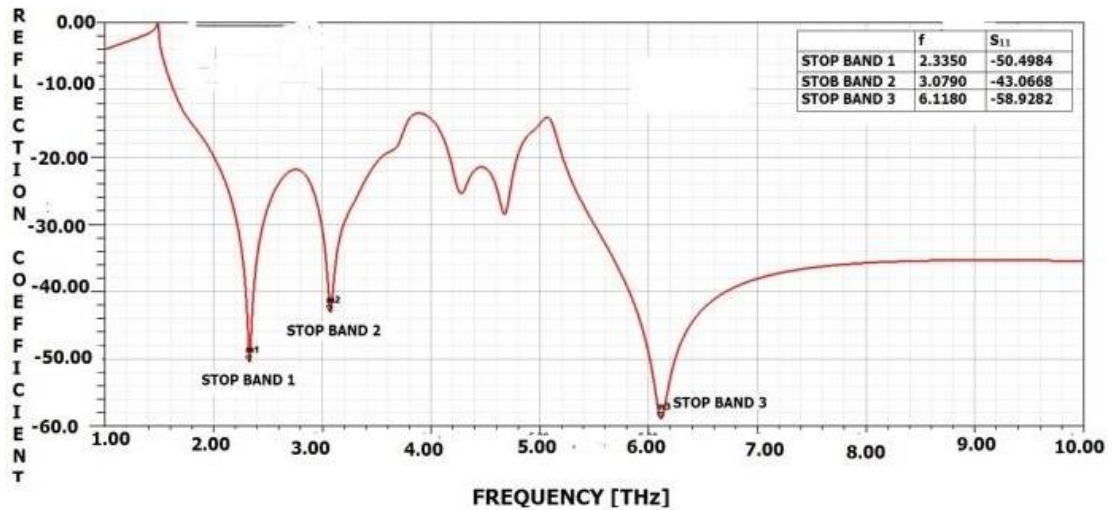


Fig. 5. Reflection coefficient (S_{11}) of SL-shaped FSS structure (color online)

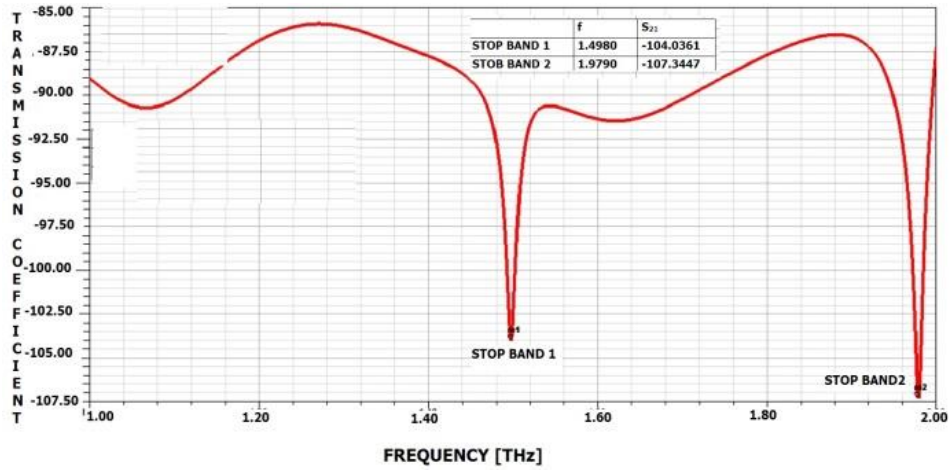


Fig. 6. Transmission coefficient (S_{21}) of SL-shaped FSS structure (color online)

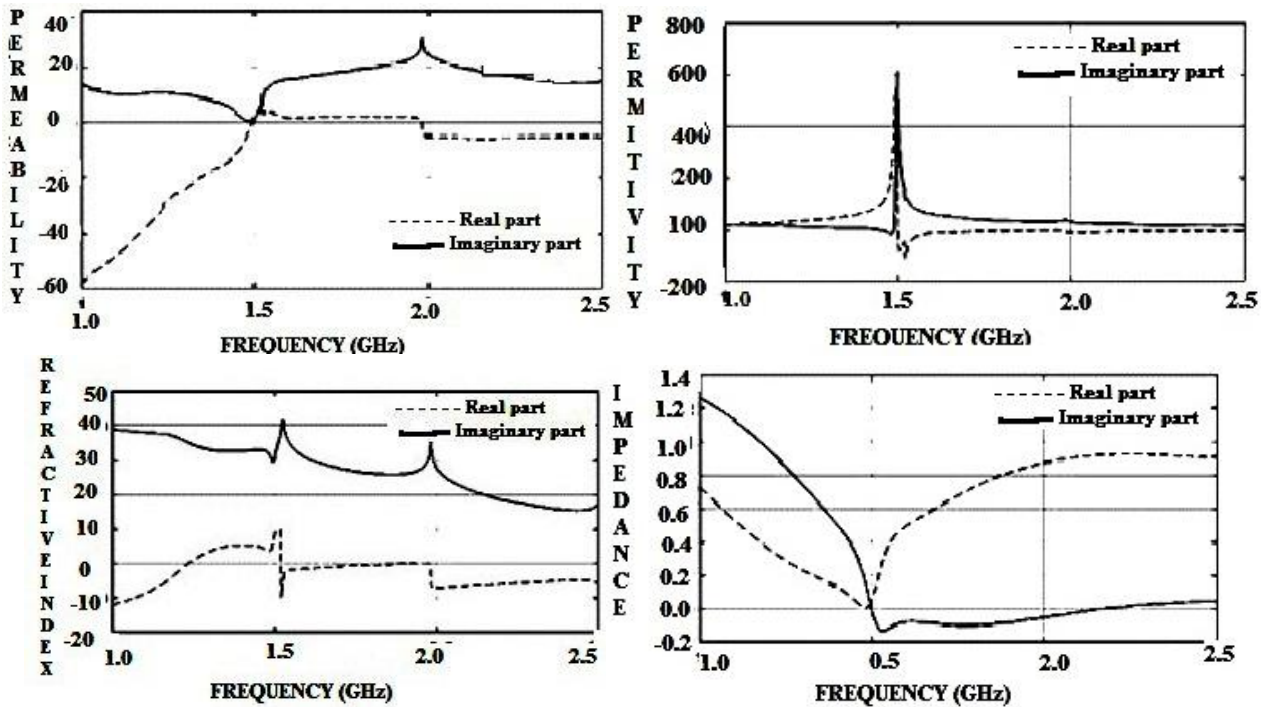


Fig. 7. Permeability, Permittivity, Refractive Index, and Impedance of SL-shaped FSS structure

4. Antenna design

4.1. Rectangular patch antenna Design

The proposed patch antenna design is illustrated in Fig. 8. The antenna top layer size is $350 \times 400 \mu\text{m}^2$ printed on silicon substrate $1000 \times 1000 \mu\text{m}^2$. The lower layer is $40 \mu\text{m}$ thick, and the array of FSS is printed on the bottom layer with $30 \mu\text{m}$ thickness as shown in Fig. 9. The geometrical configuration of the THz rectangular patch antenna printed on a substrate with an array of metallic FSSs as shown in Fig. 10.

These proposed antenna parameters are highlighted in Table 2. In [27], Selvakumar et al. analyzed various patch materials such as copper, graphene, and gold with a central operating frequency of 300 GHz and substrate materials

such as quartz, silicon, silicon dioxide, and silicon nitrate for Tera hertz antenna. In [28], Rajni et al. examined variety of substrate materials for a graphene patch antenna that operates in the 2.67–2.92 THz frequency band. From these literature studies, silicon is used as substrate material for the proposed design.

Table 2. Summary of the antenna parameters

Patch Parameters	Value (μm)
Length of the Patch (L)	350
Width of the Patch (W)	400
Length of the Substrate	1000
Width of the substrate	1000

4.2. Simulation results

This section carried out simulation results of the single element antenna compared with FSS metallic array printed on the substrate.

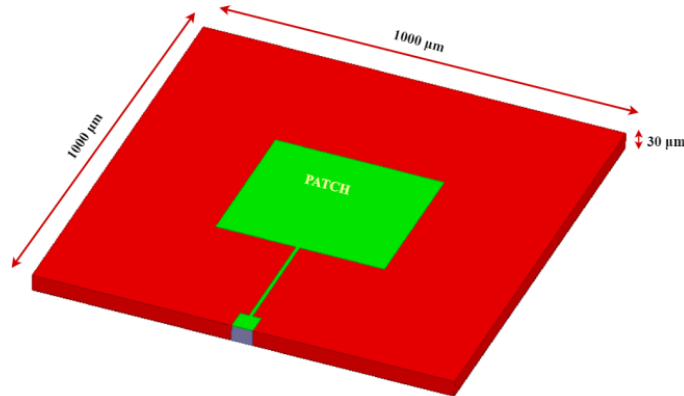


Fig. 8. Single element microstrip patch antenna (color online)

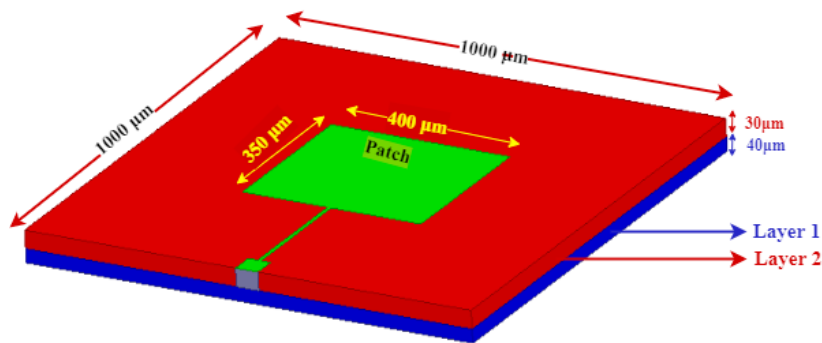


Fig. 9. Dual layer FSS-based Microstrip Patch antenna (color online)

The return loss plot of single element patch antenna and FSSs Printed antenna at resonant frequency of 1.5 THz is shown in Fig. 11. The simulation results show that FSS based microstrip patch antenna has return loss of -27.31 dB at 2.69 THz. The return loss of single element patch antenna (without FSS) is -24.98 dB at 3.17 THz. The bandwidth of

the single-layer patch antenna is 1230 GHz. Nevertheless, the bandwidth of the dual-layer using the FSS substrate is 2260 GHz. The comparison of the bandwidth plot in Fig. 12 shows that the proposed FSSs substrate antenna has much more bandwidth.

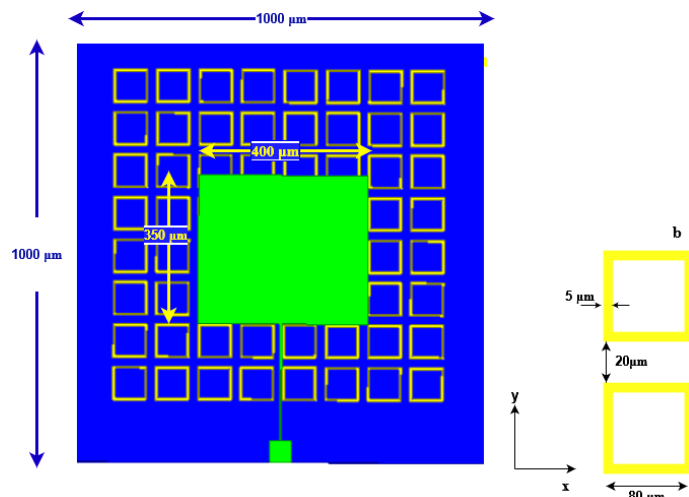


Fig. 10. The geometrical configuration of the THz rectangular patch antenna printed on a substrate with an array of metallic SRRs (color online)

Fig. 13 shows the radiation pattern of the THz rectangular patch antenna over a metamaterial substrate.

The comparison of the patch antenna with the FSS substrate is shown in Table 3.

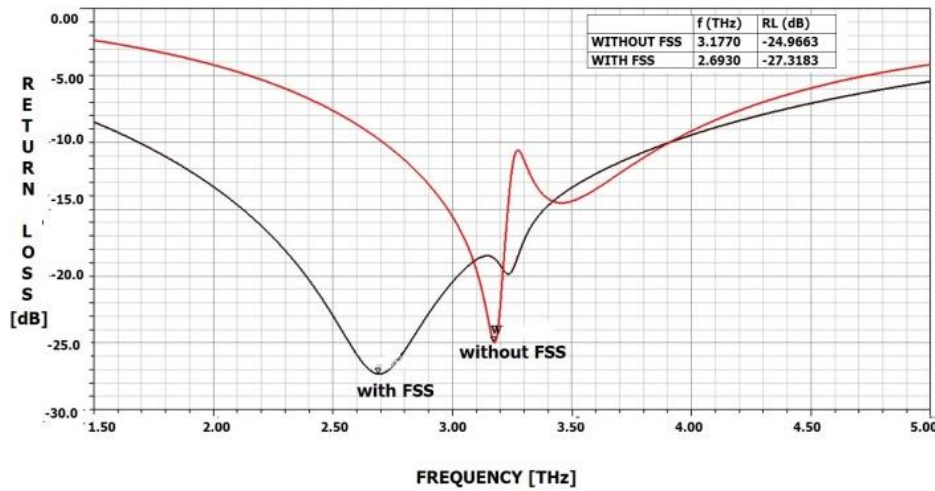


Fig. 11. Return loss plot of the single element patch antenna and FSSs Printed antenna (color online)

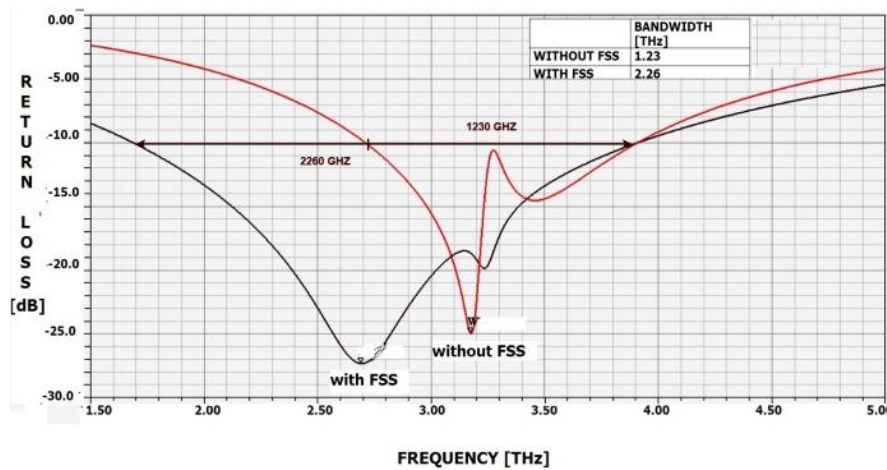


Fig. 12. Bandwidth comparison of the single element patch antenna and FSSs Printed antenna (color online)

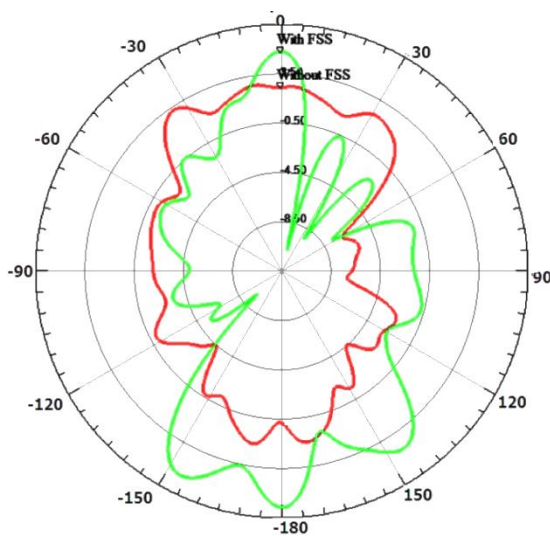


Fig. 13. The radiation pattern of the rectangular patch antenna with FSSs substrate (color online)

Table 3. Comparison results

Simulation Parameters	Single Patch Antenna	FSSs Printed Antenna
Return loss (dB)	-24.98	-27.31
Bandwidth (THz)	1.23	2.26
Directivity (dBi)	7.67	11.4
Gain (dBi)	7.93	11.67

5. Comparisons with previous research

Table 4 compares the performance of several THz microstrip antennas with the proposed dual-layer patch antenna in terms of return loss, gain, and bandwidth. Here, the various types of the patch antenna such as double T-type slot microstrip antenna [14], T-type dual-frequency microstrip antenna [15], Slotted patch RMPA [16], Microstrip antenna array [17], Stacked microstrip antenna [18], and Slotted rectangular microstrip antenna [19] were analyzed. The proposed dual-layer patch antenna covers the

range of 1.68 to 3.94 THz and the total size of this antenna is $1000 \times 1000 \times 70 \mu\text{m}^3$ which is designed over the silicon substrate. The simulation results shows that the performance of proposed FSSs based antenna is improved in terms of gain, bandwidth, and directivity when compared to other reported antennas in the related work.

6. Conclusion

In this work, the band stop FSS unit element was designed and their parameters were verified by using

MATLAB. The equivalent circuit of the FSS unit element has been modeled by using ABCD parameters. Then the proposed FSS substrate-based Terahertz antenna was compared with a single patch antenna. From the comparison, it is concluded that the proposed dual-layer FSS printed antenna has improved gain, bandwidth, and directivity. Hence, the proposed antenna is observed to be a better choice for future 6G wireless networks.

Table 4. Performance comparison of several THz microstrip antenna

References	Type of Antenna	Operating frequency (THz)	Bandwidth (GHz)	Gain (dBi)	Return Loss (dB)	Substrate material
Proposed antenna (THz)	Dual layer Microstrip Patch Antenna	2.69	2260	11.67	-27.31	Silicon
[14]	Double T-type slot microstrip antenna	0.3 and 0.76	12 and 31	7.13 and 3.71	-29 and -40	ArlonCuclad 250GT
[15]	T-type dual-frequency microstrip antenna	0.632 and 0.8702	50 and 80	Peak gain 8.2	N/A	FR-4
[16]	Slotted patch RMPA	0.703	26.4	5.235	-50.948	PBG and DGS
[17]	Microstrip antenna array	0.1	2.24	15.7	-26.04	Liquid crystal polymer
[18]	Stacked microstrip antenna	8.2	0.36	6.48	-38.85	FR-4
[19]	Slotted rectangular microstrip antenna	4.952	0.4445	4.254	-55.31	FR-4

References

- [1] X. Raimundo, M. Hajji, A. Klein, S. Salous, A. Gallant, C. Balocco, 12th Euro. Conf. Anten. & Prop. IET, 1 (2018).
- [2] Y. Li, M. Zhang, W. Zhu, M. Cheng, C. Zhou, Y. Wu, China Comm. **17**(1), 151 (2020).
- [3] S. Chen, S. Sun, G. Xu, X. Su, Y. Cai, IEEE Wireless Comm. **27**(2), 162 (2020)
- [4] L. Ma, X. Wen, L. Wang, Z. Lu, R. Knopp, China Comm. **15**(10), 86 (2018).
- [5] A. U. Zaman, S. Rahiminejad, T. Eriksson, S. Fajana, P. Enoksson, 12th Euro. Conf. on Anten. & Prop. IET, 1 (2018).
- [6] K. M. S. Huq, J. M. Jornet, W. H. Gerstacker, A. Al Dulaimi, Z. Zhou, J. Aulin, IEEE Comm. Mag. **56**(6), 94 (2018).
- [7] Han, Y. Chen, IEEE Comm. Mag. **56**(6), 96 (2018).
- [8] M. T. Barros, R. Mullins, S. Balasubramaniam, IEEE Trans. Veh. Technol. **66**(7), 5647 (2016).
- [9] K. Ntontin C. Verikoukis, IEEE Trans. on Vehi. Tech. **66**(7), 5635 (2016).
- [10] J. Federici, L. Moeller, J. Appl. Phys. **107**(1), 6 (2010).
- [11] T. Kleine-Ostmann T. Nagatsuma, J. Infr., Milli. and Terahertz Waves **32**(2), 143 (2011).
- [12] X. Yu, T. Ohira, J.-Y. Kim, M. Fujita, T. Nagatsuma, Elec. Lett. **56**(7), 342 (2020).
- [13] G. Zhang, S. Pu, X. -Y. Xu, C. Tao, J. -Y. Dun, Int. Symp. Anten. & Prop. IEEE, 1755 (2017).
- [14] H.-Y. Zhang, F.-S. Zhang, C. Wang, T. Li, Prog. Electromagn. Res. C. **73**, 167 (2017).
- [15] M. Khulbe, M. Tripathy, H. Parthasarthy, J. Dhondhiyal, Int. Conf. Comput. Intel. Comm. Net. IEEE, 191 (2016).
- [16] L. C. Paul M. M. Islam, Int. Conf. Comp. Info. Tech. IEEE, 1 (2017).
- [17] M. S. Rabbani H. Ghafouri-Shiraz, IEEE Antennas Wireless Propag. Lett. **16**, 1533 (2017).
- [18] G. S. Brar, V. Singh, E. Sidhu, Int. Conf. on Automatic control and Dynamic Optimization Tech., IEEE, 771 (2016).
- [19] G. Kaur, V. Mehta, E. Sidhu, Int. Conf. Electronics, Materials Eng. and Nano-Techn. IEEE, 1 (2017)
- [20] M. Koutsoupidou, N. Uzunoglu, I. S. Karanasiou, Int. Conf. on Bio Info. Bio Engg. IEEE, 319 (2012).
- [21] Z. Chen, X. Ma, B. Zhang, Y. Zhang, Z. Niu, N. Kuang, W. Chen, L. Li, S. Li, China Comm. **16**(2),

- 1 (2019).
- [22] N. Qasem, E. A. Aldorgam, H. Y. Alzoubi, J. Comm. Comp. **13**(2), 90 (2016).
- [23] Dawod, N. Qasem, Int. Conf. Info. Comm. Systems IEEE, 171 (2015).
- [24] N. Marcuvitz, Waveguide handbook (Electromagnetic Waves, The Institution of Engineering and Technology, 1986.
- [25] C. K. Lee, R. J. Langley, IEE Proc. H - Microwaves Optics and Antennas **132**(6), 395 (1985).
- [26] R. S. Anwar, L. Mao, Ning, Appl. Sci. **8**, (2018).
- [27] George, S., Vijayakumar, N, J. Electron. Mater. (2022); <https://doi.org/10.1007/s11664-022-09734-0>.
- [28] R. Bala, A. Marwaha, Engineering Science and Technology, an International Journal **19**(1), 531 (2016).

* Corresponding author: Selvakumargeorge@gmail.com